Journal of Applied Polymer Science

Electrical, Mechanical, Structural, and Thermal Behaviors of Polymeric Gel Electrolyte Membranes of Poly(vinylidene fluoride-*co*-hexafluoropropylene) with the Ionic Liquid 1-Butyl-3-Methylimidazolium Tetrafluoroborate Plus Lithium Tetrafluoroborate

Shalu, Sujeet Kumar Chaurasia, Rajendra Kumar Singh, Suresh Chandra
Department of Physics, Banaras Hindu University, Varanasi 221005, India
Correspondence to: R. K. Singh (E-mail: rksingh_17@rediffmail.com)

ABSTRACT: Polymeric gel electrolyte membranes based on the polymer poly(vinylidene fluoride-*co*-hexafluoropropylene) [P(VdF–HFP)] with different weight percentages of the ionic liquid (IL) 1-butyl-3-methylimidazolium tetrafluoroborate plus 0.3*M* lithium tetrafluoroborate ($LiBF_4$) salt were prepared and characterized by scanning electron microscopy, X-ray diffraction, differential scanning calorimetry, thermogravimetric analysis, Fourier transform infrared (FTIR) spectroscopy, complex impedance spectroscopy, pulse echo techniques, and Vickers hardness (*H*) testing. After the incorporation of the IL plus the salt solution in the P(VdF–HFP) polymer, the melting temperature, glass-transition temperature (T_g), degree of crystallinity, thermal stability, elastic modulus (E), and hardness (H) gradually decreased with increasing content of the IL–salt solution as a result of complexation between the P(VdF–HFP) and IL. This was confirmed by FTIR spectroscopy. A part of the IL and $LiBF_4$ were found to remain uncomplexed as well. The ionic conductivity (σ) of the polymeric gel membranes was found to increase with increasing concentration of the IL–salt solution. The temperature-dependent σs of these polymeric gel membranes followed an Arrhenius-type thermally activated behavior. © 2014 Wiley Periodicals, Inc. J. Appl. Polym. Sci. **2015**, *132*, 41456.

KEYWORDS: crystallization; differential scanning calorimetry (DSC); glass transition; ionic liquids; mechanical properties

Received 4 January 2014; accepted 26 August 2014
DOI: 10.1002/app.41456

INTRODUCTION

Researchers around the globe are focusing on ion-conducting polymer gel electrolyte membranes (generally consisting of alkali–metal salt complexes) because of their potential applications in electrochemical devices, such as batteries, fuel cells, supercapacitors, and solar cells, and high ionic conductivity (σ) at room temperature, which is equivalent to that of liquid electrolytes.[1–4] Polymeric gel membranes have high σ values, and they also offer high energy density, safe handling, ease in thin-film formation, packing flexibility, and light weight, and they provide good electrode–electrolyte contact; this makes them suitable candidates for technological applications.[5] Poly(vinylidene fluoride-*co*-hexafluoropropylene) [P(VdF–HFP)] has emerged as a promising host matrix for the preparation of polymeric gel membranes having excellent mechanical strength and electrochemical stability. Out of poly(vinylidene fluoride) (PVdF) and P(VdF–HFP) (developed by Bellcore in 1996)[6], the latter has received relatively more attention as a promising host polymer for polymer electrolytes because of its excellent mechanical strength, electrochemical stability, good hydrophobicity, better amorphous domains, and high dielectric constant (~8.4); this helps with a higher dissociation of charge carriers. The presence of the strong electron-withdrawing functional group (—C—F) in P(VDF–HFP) makes this polymer highly anodically stable. The addition of the HFP unit improves the uptake of liquid electrolytes by introducing the amorphous domain into the polymer and thereby increasing σ. The crystalline region provides enough mechanical stability to help in obtaining self-standing films. P(VdF–HFP)-based gels are optically transparent.[7–10] Therefore, the P(VdF–HFP) copolymer is considered to be a promising alternative for preparing polymer gel electrolyte membranes compared to other existing polymers.

Polymer gel electrolyte membranes based on polymers, such as poly(ethylene oxide) (PEO), poly(methyl methacrylate) (PMMA), PVdF, and polyacrylonitrile (PAN) mixed with suitable ionic salts added to low-molecular-weight organic solvents, such as propylene carbonate (PC), ethylene carbonate (EC), poly(ethylene glycol) (PEG), and dimethylformamide (DMF), as plasticizers have been reported earlier.[11–16] These polymer gel electrolytes have high σs at ambient temperature but are not mechanically stable and are

incompatible for the high-temperature range because of the volatility and flammability of the added plasticizer. Therefore, they always pose a risk for fire. On the other hand, the incorporation of ionic liquids (ILs) in polymer electrolytes is considered advantageous for the development of nonvolatile and nonflammable ion-conducting materials to improve both the safety and durability of electrochemical devices.[17] ILs are room-temperature molten salts and are mainly composed of dissociated organic/inorganic cations and inorganic anions. Several exceptional physicochemical properties of ILs, such as their inflammability, nonvolatility, excellent thermal stability, high σ up to their decomposition temperature (T_d), wide electrochemical window, good solvating capabilities, and recyclability, indicate that ILs can be useful materials for applications in electrochemical devices. Instead of using IL solutions as electrolytes, it is better to use their polymer gel electrolyte analogs to take care of the problem of leakage.[18–20] The gelation of ILs by physical or chemical techniques has attracted much attention.[21–23] Recently, the incorporation of an IL plus a salt solution (a mixture of ILs plus ionic salts) into polymer matrices has been used to prepare polymeric gel membranes having a high mechanical stability, high σ, wide electrochemical window, and wide temperature range of operation.[24,25] Bellcore[6] proposed a polymer gel electrolyte membrane based on the P(VdF–HFP) polymer for the fabrication of Li-ion batteries. Since then, interest in the polymer Li-ion battery has been focused on plasticized polymer electrolyte systems based on the P(VdF–HFP) polymer. Yang et al.[26] reported that σ reached a maximum value (2×10^{-4} S/cm) at room temperature for gel polymer electrolytes based on (1-butyl-4-methylpyridinium bis(trifluoromethanesulfonyl)imide/Lithium-bis(trifluoromethanesulfonyl)imide) B4MePyTFSI/LiTFSI/P(VdF–HFP), Navarra et al.[27] showed that an σ of about 3×10^{-4} S/cm at 50°C for Li-TFSA/*N*-butyl-*N*-ethyl pyrrolidinium (trifluoromethylsulfonyl) amide TFSA/P(VdF–HFP) was achieved, and Jung et al.[28] reported that σ values of the polymer gel membrane based on (1-butyl-1-methylpyrrolidinium bis(trifluoromethanesulfonyl) imide) PYR_{14}TFSI/LiTFSI/P(VdF–HFP) were 3.6×10^{-4} S/cm at 30°C and 5.9×10^{-4} S/cm at 50°C. However, in addition to improved σ values, safety concerns are also important for rechargeable battery applications. In this system, an IL plus lithium salt (an IL and a salt containing same the anion) were added in different amounts to the P(VdF–HFP) polymer because mixed-anion systems (i.e., a dopant salt and added IL having a different anion) have a tendency to form contact/cross-contact ion pairs, which significantly affect σ. These IL-based polymer electrolytes (in which the IL and salt have same anion) are suitable candidates for applications in rechargeable batteries.[24] Guided by our previous results[14,19] and some other similar studies,[24] we chose the IL 1-butyl-3-methylimidazolium tetrafluoroborate ($BMIMBF_4$) and the salt lithium tetrafluoroborate ($LiBF_4$) having the same anion to obtain a polymer gel electrolyte membrane. The incorporation of the IL in P(VdF–HFP) was found to enhance σ because it supplied mobile cations/anions and amorphized the polymer.[29] Therefore, it would be interesting to study such a system in the presence of a Li salt, and this could prove especially useful for applications in electrochemical devices in rechargeable batteries. In this article, we report the synthesis and structural/thermal/mechanical and electrical transport behavior of polymeric gel membranes based on P(VdF–HFP) plus IL plus a salt solution (a homogeneous mixture of IL, $BMIMBF_4$, and 0.3*M* $LiBF_4$). The question addressed in this study was whether the incorporation of the IL–salt solution in P(VdF–HFP) would change the crystallinity, thermal stability, melting temperature (T_m), σ, complexation, hardness (H), and elastic modulus (E) of the gel membranes.

EXPERIMENTAL

Materials

The starting materials poly(vinylidene fluoride-*co*-hexafluoropropylene) [P(VdF–HFP), molecular weight = 400,000 g/mol), $LiBF_4$ (purity > 99.9%) salt, and the IL $BMIMBF_4$ (purity > 99%) were procured from Sigma Aldrich (Germany). The IL was dried *in vacuum* at about 10^{-6} Torr for 2 days before use.

Synthesis of the Polymeric Gel Membranes

The polymeric gel membranes were prepared by solution casting method. $LiBF_4$ salt (0.3M) was dissolved into IL by stirring at room temperature to form IL–salt solution separately. The desired amount of the P(VdF–HFP) polymer was dissolved in acetone by stirring at 50°C until a clear homogeneous mixture was obtained. The resulting IL–salt solution was then mixed with different weight percentage ratios of a P(VdF–HFP)–acetone solution by stirring at 50°C until a homogeneous viscous solution was obtained. The resulting viscous solution was cast over a polypropylene Petri dish, and the solvent was allowed to evaporate slowly at room temperature for 24 h. The membranes were further dried at 10^{-6} Torr for 2 days to completely remove the volatile solvent. The prepared polymeric gel membranes were freestanding and optically transparent.

The surface morphologies of the polymeric gel electrolyte membranes were examined by a scanning electron microscope (model Quanta C-200). The X-ray diffraction (XRD) profiles of the polymer gel electrolytes membranes were measured by an X'Pert PRO X-ray diffractometer (PaNalytical) with Cu Kα radiation (wavelength = 1.54 Å) in the range $2\theta = 10$ to 80°.

Differential scanning calorimetry (DSC) was carried out with a Mettler DSC 1 system in the temperature range −110 to 160°C at a heating rate of 10°C/min under continuous purging of nitrogen. The Fourier transform infrared (FTIR) spectra of the polymeric gel membranes were recorded with the help of a PerkinElmer FTIR spectrometer (Model RX 1) from 3500 to 400 cm^{-1}.

The σ values of the polymeric gel membranes were measured by a complex impedance spectroscopy technique with a Wayne Kerr precision impedance analyzer (model 6500 B series) in the frequency range 100 Hz to 5 MHz. The bulk resistance (R_b) was determined from complex impedance plots. σ was calculated with the following relation:

$$\sigma = \frac{1}{R_b} \times \frac{l}{A} \quad (1)$$

where l is the thickness of the sample and A is the cross-sectional area of the sample. For temperature-dependent σ studies, disc-shaped polymeric gel membranes were placed between two stainless steel electrodes, the whole assembly was kept in a temperature-controlled oven, and the temperature was measured with a CT-806 temperature controller containing a J-type

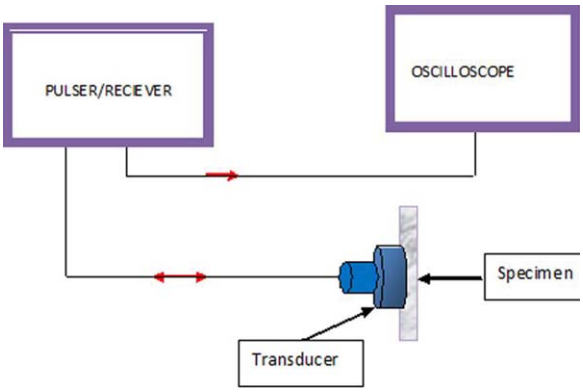

Figure 1. Schematic representation of the experimental setup of v measurement. [Color figure can be viewed in the online issue, which is available at wileyonlinelibrary.com.]

thermocouple. The σ of pure IL was measured by a conductivity cell consisting of two stainless steel plates (area $\approx$ 1.0 cm^2) separated by 1 cm. The viscosity of the IL was measured by a Brookfield DV-III Ultra rheometer in the temperature range -10 to 80°C. The instrument was calibrated with a standard-viscosity fluid supplied by the manufacturer before each measurement. To see the effect of the IL–salt solution in P(VdF–HFP) on the mechanical stability of the resulting membranes, the bulk elastic modulus (E) E of the prepared polymeric gel membranes was measured at room temperature.

A pulse technique was used for the determination of E; this involved the measurement of ultrasonic velocity (v). A pulser/receiver (Olympus model 5900PR) sent the radio frequency pulse to excite a 6-MHz piezoelectric transducer (D6HB-10) to generate longitudinal ultrasonic waves (see Figure 1). The transducer was used for both transmitting and receiving ultrasonic waves and was coupled to the disc-shaped membrane (thickness $\approx$ 1.23 mm). The return echo was received by the pulser/receiver. The echo pulse and the input pulse were displayed on a 500-MHz Agilent digital storage oscilloscope DSO5052A. The transit time of the echo pulse was recorded, and v could be calculated ($v = 2d/t$) from this value. The E values of the samples were calculated with the relation $E = v^2\rho$, where v is the velocity of the longitudinal wave and ρ is the density of the samples. ρ was determined by the division of the mass of the dried samples by the volume.

Microindentation measurements were performed on the specimen with an automated digital Vickers microhardness tester (Vaiseshika Electron Devices, model DHV-1000). In this study, the evolution of the H behavior due to load was investigated by instrument indentation with a 50-g load. The indented mark was examined with both optical photography and computer-operated software. The H number measurement was carried out at room temperature.

RESULTS AND DISCUSSION

Changes in the Crystalline Nature of P(VdF–HFP) due to IL–Polymer Interactions

The incorporation of the IL–salt solution into the P(VdF–HFP) polymer or vice versa led to changes in the crystalline nature of the polymer as a result of ion–polymer interactions. We studied

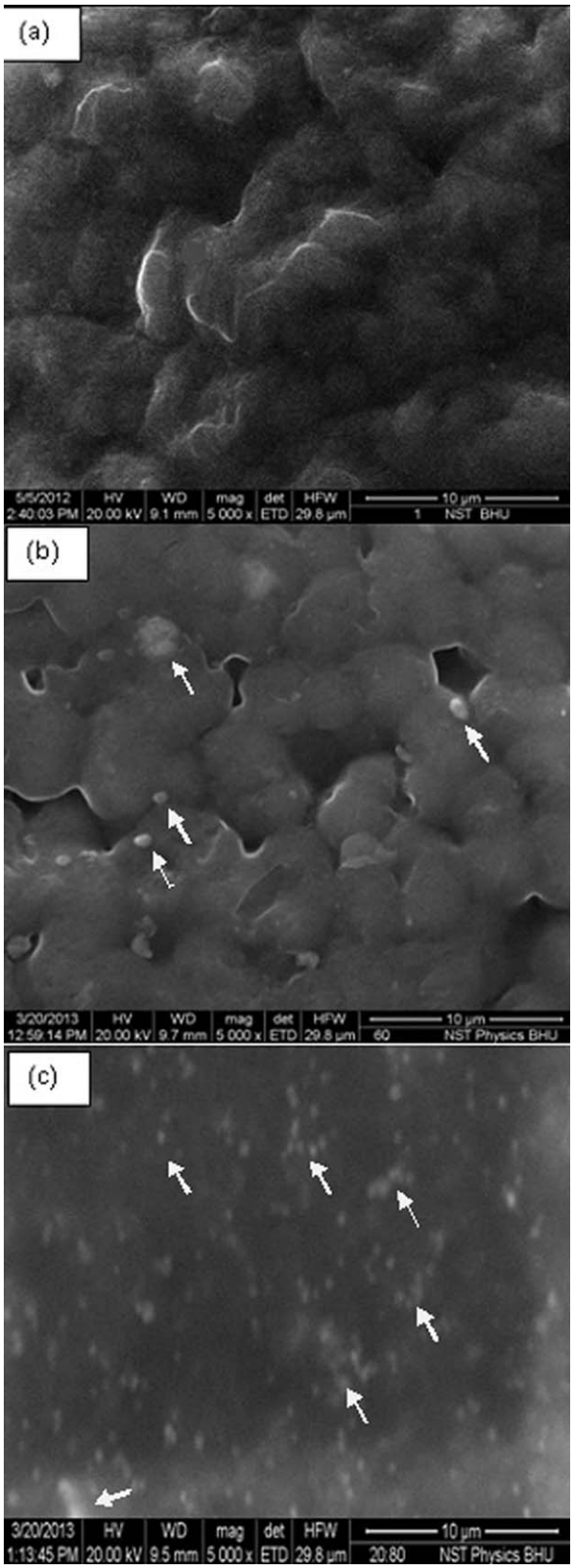

Figure 2. SEM micrograph for (a) P(VdF–HFP), (b) P(VdF–HFP) plus 60 wt % IL–salt solution, and (c) P(VdF–HFP) plus 80 wt % IL–salt solution gel membranes.

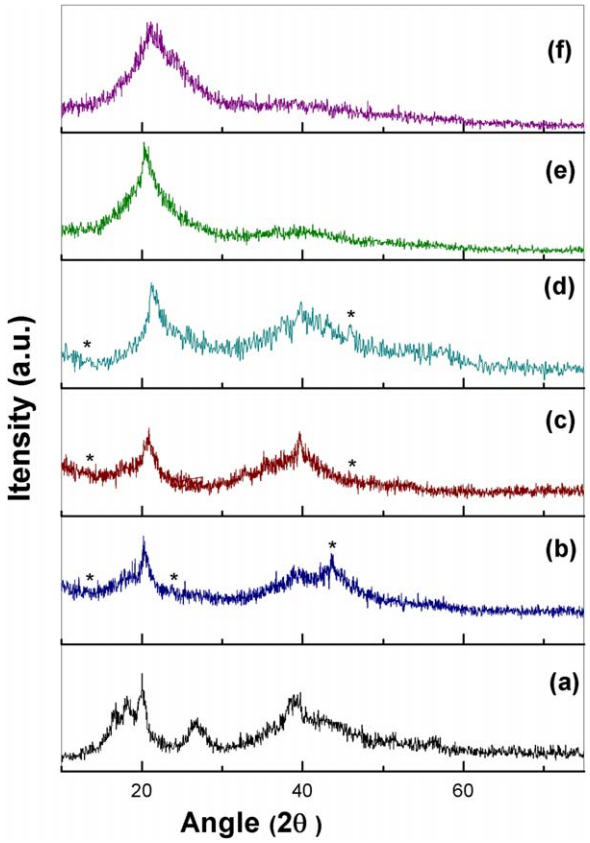

Figure 3. XRD profiles of the (a) pure P(VdF–HFP), (b) P(VdF–HFP) plus 20 wt % salt and P(VdF–HFP) + x wt % IL–salt solution gel membranes for x = (c) 20, (d) 40, (e) 60, and (f) 80. [Color figure can be viewed in the online issue, which is available at wileyonlinelibrary.com.]

this by using a variety of techniques, including scanning electron microscopy (SEM), XRD, DSC, and FTIR spectroscopy. Crystalline grains of the P(VdF–HFP) membrane were observed, as shown in Figure 2(a). On incorporation of the 20 wt % IL–salt solution in the P(VdF–HFP) polymer, the size of the grains decreased [see Figure 2(b)]. We observed some white crystallites (marked by arrows), which were not present in the pristine P(VdF–HFP) [Figure 2(a)] that could be assigned to the coexistence of the uncomplexed $LiBF_4$ salt. Furthermore, on higher loading of the IL–salt solution, say 80%, the membrane became more amorphous with no crystalline polymer grains [Figure 2(c)]. In this case also, many separated out crystallites were present. Our DSC and XRD results, described later, confirmed that these crystallites were those of $LiBF_4$.

The XRD profile of the pure P(VdF–HFP), P(VdF–HFP) plus $LiBF_4$ salt, and P(VdF–HFP) + x wt % IL–salt solution gel membranes containing different amounts of IL–salt solution are shown in Figure 3. The diffraction profile of the pristine P(VdF–HFP) consisted of a broad halo at $2\theta = 20$ and 38°, over which crystalline peaks were present at $2\theta = 18.21$ 20.04, 26.71, and 38.83° [see Figure 3(a)]. These peaks were also reported by Abbrent et al.[30] and Saikia et al.[31] and were due to the crystalline phase of α-PVdF. The simultaneous presence of the halo and crystalline peaks confirmed partial crystallization or an overall semicrystalline morphology for P(VdF–HFP). On loading the IL–salt solution in the P(VdF–HFP) polymer, the crystalline peaks at 18.21, 26.71, and 38.83° disappeared or became less intense, and only one broad peak/halo at $2\theta = 20°$ remained. The broadening of the halos in the case of the P(VdF–HFP) plus IL–salt solution gel membranes indicated the decrease in the crystallinity/or increase in the amorphicity of the P(VdF–HFP) polymer, which helped with the enhancement of σ.[32] In the earlier paragraph, while discussing the SEM of various membranes, we concluded that $LiBF_4$ crystallites were present in the SEM micrographs. The presence of the crystallites was also confirmed by XRD analysis. The $LiBF_4$ salt had prominent peaks at $2\theta = 14$, 21, 23, 26, 28, 32, 39, and 44°.[33] Some of these peaks were observed in the XRD profile of the P(VdF–HFP) plus 20 wt % $LiBF_4$ polymer electrolyte membrane without IL [as marked by the asterisk in Figure 3(b)]. These peaks were drowned in the broad halos and were less prominent in the IL-containing polymer electrolyte membranes. This effect was more visible in higher IL-loading samples [see Figures 3(c–f)].

The DSC thermograms of the pure P(VdF–HFP) [see Figure 4(a)] showed the characteristic semicrystalline to amorphous phase-transition peak marked with $T_m \approx 145$°C and $T_g \approx -35$°C. As shown in Figure 4, when the amount of added IL–0.3M $LiBF_4$ salt in the polymer increased, we observed shifts in T_m, the melting-related peak broadened, and the glass-transition temperature (T_g) related peak also shifted. Furthermore, we noted that an additional phase-transition peak (T_1) at about 107°C appeared. The implications of these observations and the conclusion drawn are discussed later:

1. The addition of IL (which could act as a plasticizer) was expected to decrease the degree of crystallinity (X_c). X_c could be calculated from the area under melting [which was a measure of melting heat (ΔH_m) involved in the phase transition] from the knowledge of the melting heat of 100% crystalline P(VdF–

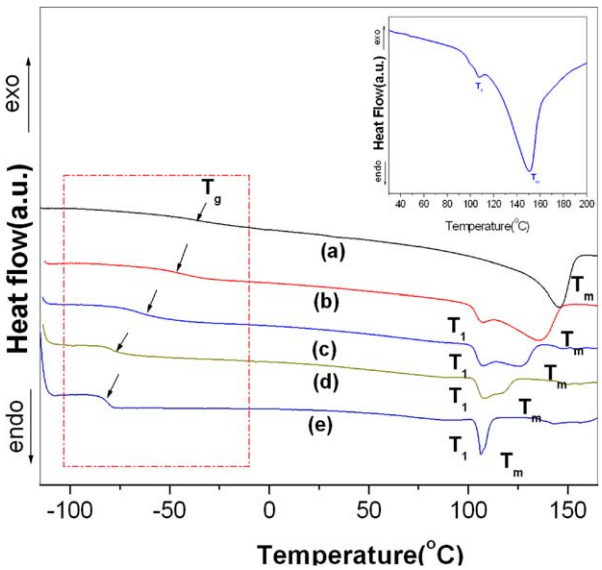

Figure 4. DSC thermograms for (a) P(VdF–HFP) and P(VdF–HFP) + x wt % IL–salt solution gel membranes for x = (b) 20, (c) 40, (d) 60, and (e) 80. The inset shows the DSC thermogram of P(VdF–HFP) plus 5 wt % $LiBF_4$ salt. [Color figure can be viewed in the online issue, which is available at wileyonlinelibrary.com.]

Table I. T_m, T_g, Enthalpy (ΔH), and X_c of the P(VdF–HFP) + x wt % IL–Salt Solution Gel Membranes for Different Values of x Obtained by DSC

Sample	T_g (°C)	T_1 (°C)	T_m	ΔH (J/g)	X_c (%)[a]
Pure P(VdF-HFP)	−35	107	145	36.02	34
P(VdF-HFP) + 20 wt % $BMIMBF_4$ + 0.3*M* $LiBF_4$	−45	107	135	27.03	26
P(VdF-HFP) + 40 wt % $BMIMBF_4$ + 0.3*M* $LiBF_4$	−62	107	126	15.08	14
P(VdF-HFP) + 60 wt % $BMIMBF_4$ + 0.3*M* $LiBF_4$	−77	107	117	7.09	6
P(VdF-HFP) + 80 wt % $BMIMBF_4$ + 0.3*M* $LiBF_4$	−81	105	108	4.39	4
P(VdF-HFP) + 5% $LiBF_4$		107	150	41.5	39.6

[a] Estimated from DSC measurement (%).

HFP) (ΔH_m^o). The value of $\Delta H_m{}^o$ was 104.7 J/g.[34] The ratio of ΔH_m to ΔH_m^o gives X_c:

$$X_c = \frac{\Delta H_m}{\Delta H_m^o} \times 100 \quad (2)$$

The value of ΔH_m and X_c are given in Table I. The result clearly shows that X_c decreased from 34 to 4%.

2. T_g decreased from −35 to −81°C, whereas T_m changed from 145 to 119°C as more and more IL was incorporated. The phase-transition temperature, T_g, and T_m of polymers are directly related to their chain flexibility and/or X_c. So, it is very important to study the T_g because it marks the transition between brittle or hard properties at lower temperature to rubbery behavior or flexibility at high temperatures. The T_g of the polymer decreased with increasing concentration of the IL; this reduced the intermolecular forces between the IL and polymer and enhanced the segmental motion of the polymer network. Because of the plasticization effect of IL,[14,19,23] the T_g of the polymer was reduced by the addition of IL. Unlike conventional plasticizers (EC, PC, etc.), the IL did not degrade mechanical integrity in the polymeric membranes. Scott et al.[35] used the IL 1-Buty-3-methylimidazolium hexafluorophosphate ($BMIMPF_6$) as a plasticizer for the polymer PMMA and found that PMMA could be used in broad range of temperatures when IL was incorporated into it. The negligible vapor pressure and outstanding thermal stability of the IL made it a better plasticizer.

3. In the DSC, an unexpected peak at $T_1 \approx 107$°C appeared; this did not shift with increasing concentration of IL–salt solution in the polymeric gel membranes. This peak, therefore, was possibly not related to polymer and may have been related to the phase transition of the $LiBF_4$ salt. We performed DSC for the membrane (without IL) consisting of P(VdF–HFP) plus $LiBF_4$ salt (see inset in Figure 4) only, and we again found a peak at about 107°C apart from the peak of P(VdF–HFP); this clearly confirmed that this peak was related to the $LiBF_4$ salt. The phase transition in $LiBF_4$ at nearly this temperature was reported earlier by Reynhyrdt and Lourens[36] from NMR studies. The SEM and XRD results discussed earlier also showed the presence of $LiBF_4$ crystallites in the membrane.

Change in the Thermal Stability of P(VdF–HFP) due to the Presence of IL

The thermal stability of the pure IL ($BMIMBF_4$), pure P(VdF–HFP), pure salt $LiBF_4$ (IL–salt solution), and P(VdF–HFP) + x wt % (IL–salt) solution polymeric gel membranes were investigated by thermogravimetric analysis (TGA). The TGA and their derivative thermogravimetric analysis (DTGA) curves are shown in Figure 5. The thermograms showed that the weight loss peak (T_d) due to the decomposition occurred at 475°C for pristine P(VdF–HFP), at 470°C for pure IL, and at 300°C for pure $LiBF_4$. In the presence of salt, the IL decomposed at 457°C; this indicated an IL–salt interaction. The IL (and/or salt) also changed the T_d of P(VdF–HFP). At a low IL–salt solution concentration (20%), the amount of IL was small, and hence, the peak associated with it at about 455°C was negligibly small, but the T_d of P(VdF–HFP) shifted to 383°C from 475°C (Figure 5). When the IL–salt solution concentration went to 40%, the T_d of IL was clearly observed at 433°C, whereas the T_d of P(VdF–HFP) was shifted at about 380°C. When a very large amount of IL–salt solution was present, the peak related to the T_d of P(VdF–HFP) became small, whereas the decomposition peak of the uncomplexed IL at 455–460°C was dominant. Close observation of Figure 5(g,h) showed us that there were three peaks at 325, 377, and 455°C and 305, 373, and 460°C, respectively, for membranes with 60 and 80% IL–salt solution. The three peaks were possibly due to the polymer–IL complex, uncomplexed polymer, and uncomplexed IL.[37] Liew et al.[38] reported that the polymer gel electrolyte based on the P(VdF–HFP)/lithium perchlorate salt ($LiClO_4$)/1-butyl-3-methylimidazolium chloride IL was thermally stable up to 232°C. However, in this case, it may be remarked here that no component was volatile within these membranes, as there was no weight loss when they were heated from room temperature to 350–400°C. This well confirmed that the thermal stability of the prepared polymeric gel membranes for application in lithium-ion batteries would be safe even at higher temperatures.

IL–Polymer Interaction as Studied by FTIR Spectroscopy

FTIR spectroscopy was used to investigate possible ion–polymer interactions and to identify the conformational changes in the host P(VdF–HFP) polymer matrix with the addition of the IL ($BMIMBF_4$), $LiBF_4$ salt, and IL–salt solution ($BMIMBF_4$/$LiBF_4$) in it. The important peaks related to crystalline and amorphous P(VdF–HFP) were in the region 1000–400 cm^{-1}, whereas the most important C—H-related vibration of the IL imidazolium cation ring (which was expected to interact with the polymer) and its butyl chain were in the region 3300–2800 cm^{-1}. The FTIR spectra of the pure P(VdF–HFP), pure IL, IL–salt solution, and P(VdF–HFP) plus x wt % IL–salt solution (where $x = 20$, 40, 60, and 80) in the two regions of interest, namely,

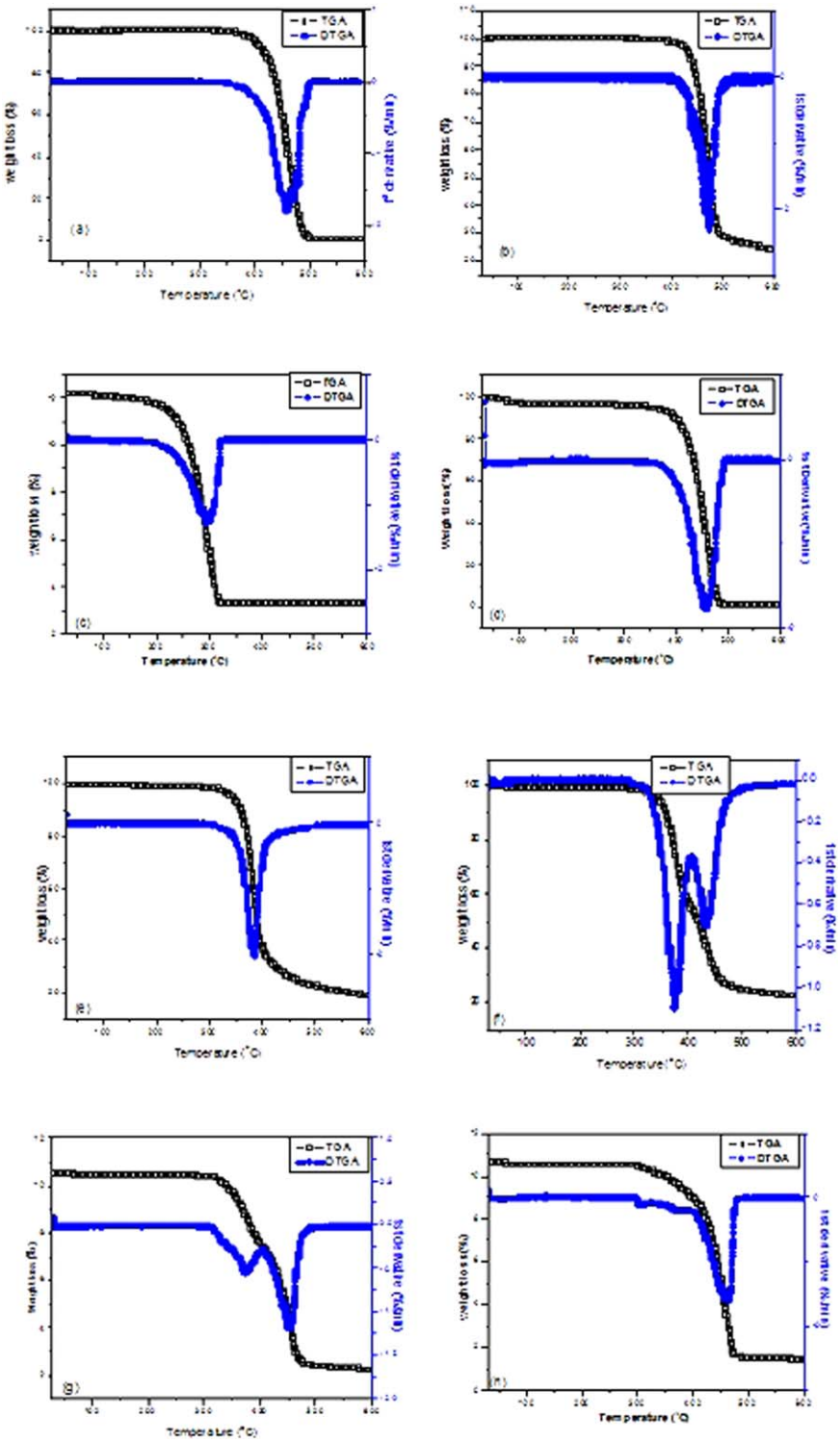

Figure 5. TGA and DTGA curves for the (a) pure IL, (b) pure P(VdF–HFP), (c) pure $LiBF_4$ salt, (d) IL–salt solution, and P(VdF–HFP) + x wt % IL–salt solution gel membrane for x = (e) 20, (f) 40, (g) 60, and (h) 80. [Color figure can be viewed in the online issue, which is available at wileyonlinelibrary.com.]

1000–400 and 3300–2800 cm^{-1} are shown in Figure 6(a) and 6(b), respectively, and their assignments are listed in Table II. The occurrence of any interaction between P(VdF–HFP), IL, and IL–salt solution led to changes in the frequency of the vibrational band and/or changes in the relative intensities or appearance of new vibrational bands. Some distinct changes were observed, and are discussed later, when the IL and IL–salt solution were entrapped in the P(VdF–HFP) polymer matrix; this indicated some possible conformational changes in the host polymer.

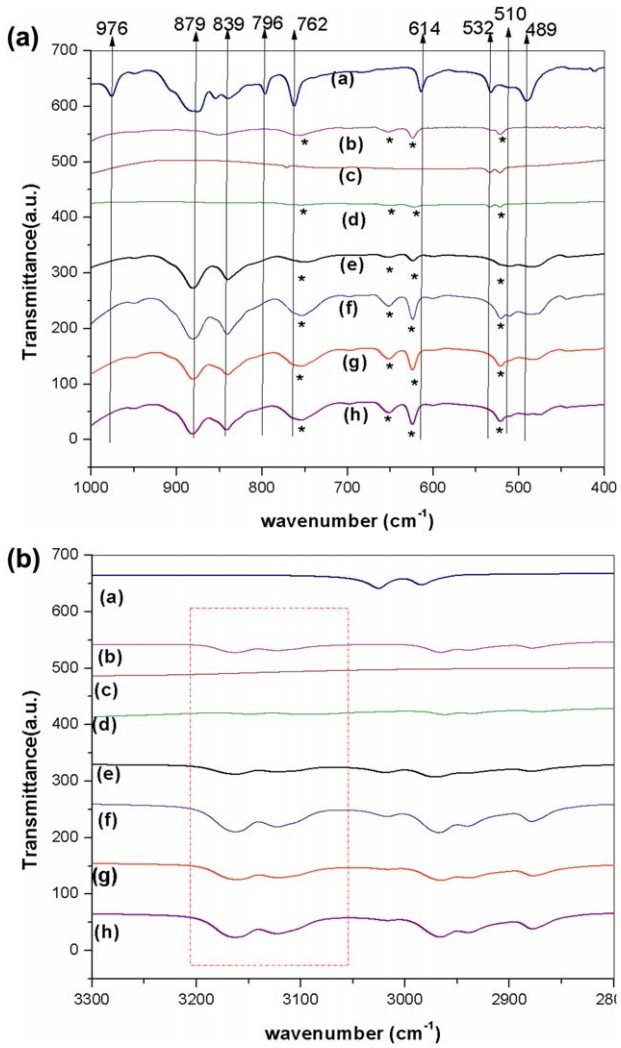

Figure 6. **(a)** FTIR spectra of the (a) pure P(VdF–HFP), (b) pure IL, (c) pure $LiBF_4$, (d) IL–0.3*M* $LiBF_4$ and P(VdF–HFP) + *x* wt % IL–salt solution gel membrane for *x* = (e) 20, (f) 40, (g) 60, and (h) 80 in the region 1000–400 cm^{-1}. **(b)** FTIR spectra of the (a) pure P(VdF–HFP), (b) pure IL, (c) pure $LiBF_4$, (d) IL–0.3*M* $LiBF_4$, and P(VdF–HFP) + *x* wt % IL–salt solution gel membrane for *x* = (e) 20, (f) 40, (g) 60, and (h) 80 in the region 3300–2800 cm^{-1}. [Color figure can be viewed in the online issue, which is available at wileyonlinelibrary.com.]

The intense bands of P(VdF–HFP) appearing at 489, 532, 614, 762, 796, 839, 879, and 976 cm^{-1} were of particular interest to us because the intensity of other bands was low and/or overlapped with the bands of the pure IL and IL plus salt solution. The characteristic vibrational bands observed at 489, 532, 614, 762, and 976 cm^{-1} corresponded to the crystalline phase (α phase) of the P(VdF–HFP) polymer, whereas the bands related to the amorphous phase (β phase) of the polymer were observed at 879 and 839 cm^{-1}. We noted that the peaks appearing at 976 cm^{-1} [due to the C—F stretching vibration of the P(VdF–HFP) polymer] at 614 cm^{-1} (due to mixed-mode CF_2 bending), 532 cm^{-1} (due to the bending and wagging vibrations of the CF_2 group), and 796 cm^{-1} [due to the CF_3 stretching vibrational mode of the P(VdF–HFP) polymer] disappear after the addition of IL or IL–salt solution. We also observed that the peak at 489 cm^{-1} (due to bending and wagging vibrations of the CF_2 group) shifted downward with the addition of IL or IL–salt solution. Furthermore, the intensity of the peak corresponding to the band at 879 cm^{-1}, which was assigned to the amorphous phase (β phase) of the P(VdF–HFP) polymer, increased. These observations clearly indicated conformational changes observed in the P(VdF–HFP) polymer after complexation with the cation of the IL or IL–salt solution.[39–42]

Several prominent peaks associated with the imidazolium cation [1-butyl-3-methylimidazolium ($BMIM^+$)] observed at 623, 653, 755, 849, 1174, 1467, 1573, 1748, 2878, 2939, 2965, 3075, and 3225 cm^{-1} are listed with their assignments in Table II. Most of the bands showed no shift when $LiBF_4$ salt was dissolved in IL or the IL–salt solution was entrapped in the host polymer [Figure 6(a), marked with an asterisk]. Some of the $BMIM^+$ related peaks overlap with the bands of host P(VdF–HFP) polymer. We also observed that the peak appearing at 762 cm^{-1} due to the CH_2 rocking vibrations of the pure P(VdF–HFP) was near the peak of IL at 755 cm^{-1}. The peaks at 854 and 839 cm^{-1} were very near the peak of IL at about 849 cm^{-1}. The peak at 2965 cm^{-1} could not be clearly seen because it was near the peak of the polymer chain vibrations at 2983 cm^{-1}, and the peaks at about 2878 and 2939 cm^{-1} did not shift with the increasing concentration of IL–salt solution [see Figure 6(b)]. This suggested that the butyl chain did not complex with the polymer backbone.[29,43–45]

To observe the complexation of the imidazolium cation ring, we focused our attention on the spectral range 3230–3070 cm^{-1}, which was related to the C—H stretching vibrational modes of the imidazolium ring. The antisymmetric and symmetric stretching vibrational modes of HC(4)—C(5)H of the pure IL ($BMIMBF_4$) occurring at 3122 and 3163 cm^{-1}, respectively, and a weak shoulder appearing around 3104 cm^{-1}, which was assigned to the stretching vibrational mode of C(2)—H,[45] were also observed. Stabilization due to H-bonding interactions between the cation and anion was found to be greater in the case of interactions involving C2—H because C2 was positive because of the electron-deficient π-bond formation of the C=N bond. On the other hand, C4 and C5 were neutral because of π-bond formation between two carbons equally sharing the available electrons; this offered less stabilization.[46–50]

The expanded spectra are shown in Figure 6(b), and the deconvoluted peaks are shown in Figure 7. In all cases, the deconvolution was carried out with multi-Gaussian peaks to extract the exact peak positions of the P(VdF–HFP) plus IL–salt solution gel membranes. Figure 7 shows the deconvoluted spectra of the pure IL and P(VdF–HFP) plus *x* wt % IL–salt solution (with the values of the square of the regression coefficient of about 0.999). As shown in Figure 7(a), it was clear that the deconvoluted FTIR spectrum of the pure IL consisted of a strong peak at 3163 cm^{-1} (labeled as X_1) and two relatively less intense peaks at 3104 and 3124 cm^{-1}. The deconvoluted spectrum of P(VdF–HFP) + *x* wt % IL–salt solution gel membranes consisted of two peaks at 3175 cm^{-1} (labeled as X_2 in Figure 7) and 3159 cm^{-1} (labeled as X_1 in Figure 7). From Figure 7, we concluded that there was a simultaneous presence of complexed (peak labeled as X_2) and uncomplexed (peak labeled as X_1) ILs

Table II. Possible Assignment of Some Significant Peaks in the FTIR Spectra of the Pure P(VdF–HFP) and Pure IL $BMIMBF_4$

Sample	IR bands (cm^{-1})	Assignment
Pristine P(VdF-HFP)	489, 532	Bending and wagging vibrations of the CF_2 group
	614	Mixed mode of CF_2 bending and CCC skeletal vibration
	762	CH_2 rocking vibration
	796	CF_3 stretching vibration
	839	Mixed mode of CH_2 rocking
	879	Combined CF_2 and CC symmetric stretching vibrations
	976	C-F stretching
	2983, 3024	Symmetric and antisymmetric stretching vibrations of CH_2
$BMIMBF_4$	623	Imidazole ring vibration
	653	Imidazole C—N—C bending
	755	Out-of-plane imidazole C—H bending and stretching of BF_4^- anions
	849	In-plane imidazole ring bending
	1028, 1135	Stretching vibrations of the B—F bond in BF_4
	1174	Imidazole H—C—C and H— C—N bending
	1573, 1467	Imidazole ring stretching
	1748	Imidazole —C=N— bending
	2878, 2939	C—H stretching of the butyl chain
	2965	Antisymmetric stretching mode of CH_3
	3075, 3225	C—H stretching vibrations of the imidazolium cation ring
BF_4^-	520	BF_4^- anion

in the P(VdF–HFP) plus IL–salt solution gel membranes. As we increased the IL–salt solution content, the peak at 3175 cm^{-1} shifted to about 3175, 3174, 3172, and 3172 cm^{-1} for $x = 20$, 40, 60, and 80, respectively. Figure 8 shows the ratio of the relative intensities of uncomplexed to complexed IL (X_1/X_2). As shown in Figure 8, we also observed the X_1/X_2 intensity ratio increased with the concentration of the IL–salt solution. As shown in Figure 8, we concluded that at a lower concentration of added IL–salt solution in the polymer gel membrane, most of the IL complexes with the polymer and less uncomplexed IL was entrapped in the matrix. As the concentration of IL–salt solution in the polymer gel membrane increased, the amount of uncomplexed IL increased; this led to an increase in the relative intensity of the X_1 peak.

Role of IL in Changing the Mechanical Properties (*E* and *H*) of the Polymeric Membranes

E was evaluated from *v* as measured by a pulse echo technique, as discussed earlier in the Experimental section. The values of *v*, bulk modulus *E*, and ρ are given in Table III. ρ did not change much, but *v* changed with the change in the flexibility of the membranes because of amorphicity. *E* decreased with increasing amount of IL–salt solution in the polymeric gel membranes (see Table III). This was due to the plasticization effect of the IL, which made the polymers more flexible. This result suggests that the IL acted as a plasticizer and enhanced the polymer chain flexibility.

Another important mechanical property of materials is *H*, which is correlated with *E* because both of them depend on the material structure and their intramolecular and intermolecular interactions.[51] *H* is a measure of the resistance to various kinds of shape changes upon the application of forces. Benavente et al.[52] and Sacristán et al.[53] proposed a power relation between *H* and *E* for copolymers of ethylene–α-olefins, that is, $H = aE^b$, where *a* and *b* are constants. A proportional dependence relation (i.e., $H = E/10$) was proposed by Flores et al.[54] for polymers and glasses, a linear relation (i.e., $E = 15H$) was given by Boycheva et al.[55] The indentation *H* is a measure of the resistance to material deformation due to a constant compression load from a sharp object. The Vickers *H* test method consists of indenting the test material with a diamond indenter with a square base and an angle of 136° between opposite faces subjected to a load. The two diagonals of the indentation left in the surface of the material after the removal of the load are measured with a microscope, and their average is calculated. The area of the sloping surface of the indentation is calculated. The Vickers *H* is obtained by division of the load by the area of indentation (in square millimeters). Figure 9 Shows the Vickers *H* images of the pure P(VdF–HFP) and P(VdF–HFP) + *x* wt % IL–salt solution gel membranes with a load of 50 g for 15 s. The *H* values for the pure P(VdF–HFP) and P(VdF–HFP) plus 20 wt % IL–salt solution gel membranes were 37.65 and 33.8 Kgf/mm^2, respectively. However, we were not able to measure the *H* value for the higher loading (80 wt %) IL–salt solution [see Figure 9(c)] because we failed to capture the indent because of the very small recovery time of the membrane containing higher amount of IL–salt solution, and hence, the indentation mark was quickly erased before they could be photographed. Nonetheless, from the previous limited data, *H* of the polymeric gel membrane was found to decrease with increasing concentration of IL–salt solution. The decrease in *H* with increasing concentration of the IL–salt solution was also related to the decrease in *E* of the polymeric gel membranes, as evident from the ultrasonic study. This was qualitatively in agreement with the relations between *H* and *E* of polymeric materials discussed earlier.

Ionic Transport Study

Figure 10 shows the variation in σ and viscosity of the IL–salt solution with temperature. The σ value of IL–0.3*M* $LiBF_4$ at 30°C was 4.56×10^{-3} S/cm; this value increased with temperature and made the complex a suitable electrolyte for the fabrication of solid-state-rechargeable batteries. When the Li salt content was increased further, the recrystallization of $LiBF_4$ occurred because of the formation of ion pairs between Li^+ and tetrafluoroborate (BF_4^-). As determined by the XRD analysis, recrystallization occurred when there was a high amount of $LiBF_4$ salt on the surface of polymer. We found that the solubility of Li salt in the IL incorporating the same anion was much

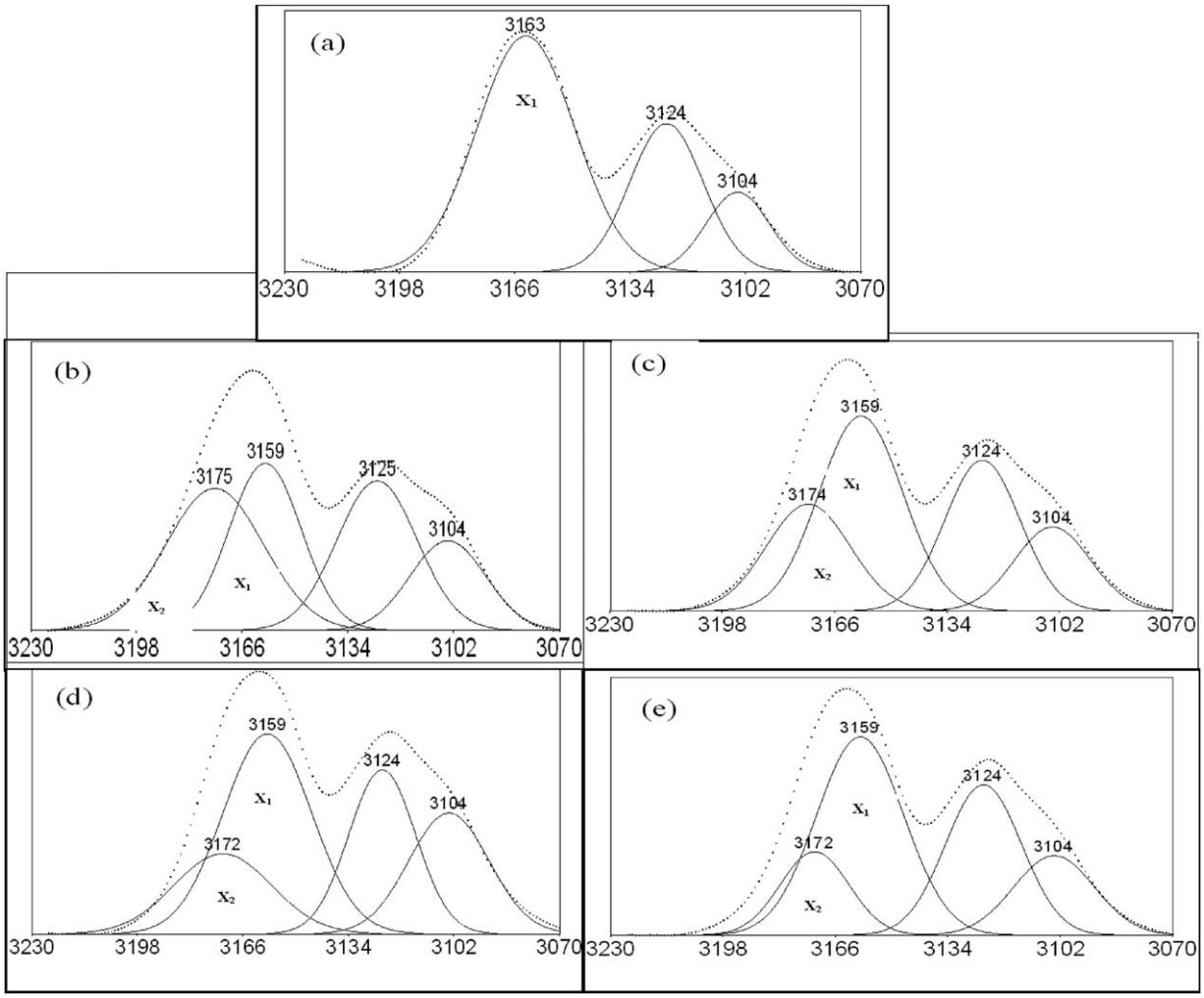

Figure 7. Deconvoluted FTIR spectra of the (a) pure IL and P(VdF–HFP) + x wt % IL–salt solution gel membranes for x = (b) 20, (c) 40, (d) 60, and (e) 80 for C—H stretching vibrational mode of the imidazolium cation ring of IL in the region 3230–3070 cm^{-1}.

higher than the system with different anions.[24] In the same anion system, chances of cross-contact ion pair formation was less; this led to a monotonic increase in σ of the IL-based polymer electrolyte system.[23] However, for an IL-based polymer electrolyte system with an IL and dopant salt having different anions, because of cross-contact ion-pair formation at intermediate IL contents, the σ usually decreases.[14,19]

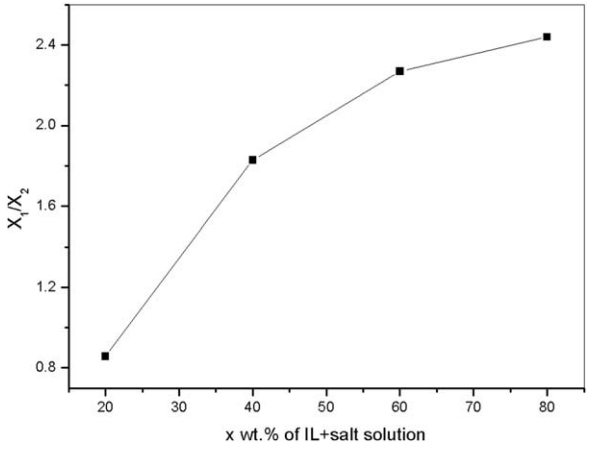

Figure 8. Ratio of the relative intensities of uncomplexed to complexed ILs (X1/X2) versus the concentration of IL-salt solution in the P(VdF−HFP) +xwt % IL-salt solution gel membranes for different values of x.

We found that as the amount of IL–salt solution increased, σ of the polymeric gel membranes increased (see Figure 13, shown later). This increment in σ was closely related to the decrease in the viscosity with temperature as they were inversely related to each other. Salminen et al.[56] (see Figure 10) also reported maximum σ for the $BMIMBF_4$ system at 0.3M $LiBF_4$. Kumar et al.[57] also found that a gel electrolyte containing 0.3M Lithium trifluoromethanesulfonate (LiTf) in 1-ethyl-3-methylimidazolium trifluoromethanesulfonate (EMITf)/P(VdF–HFP) showed the maximum room-temperature σ.

The σ of polymeric gel membranes is given as follows:

$$\sigma = \sum_i n_i q_i \mu_i \quad (3)$$

where n is the number of charge carriers, q is the charge of ions, and μ is the mobility of ions. On the basis of the previous equation, σ depends on n and the mobility of the charge carriers. As we increased the content of IL–salt solution in the polymer matrix, n increased, and this resulted in an increase in σ.

Table III. v and Bulk E Values of P(VdF–HFP) + x wt % (IL + Salt Solution) Gel Membranes for Different Values of x Obtained by Ultrasonic Measurement

Sample	ρ (g/cm^3)	v (m/s)	E (dyne/cm^2)
Pure P(VdF–HFP)	1.29	3360	14.56×10^{10}
P(VdF–HFP) + 20 wt % $BMIMBF_4$ + 0.3*M* $LiBF_4$	1.30	3083	12.36×10^{10}
P(VdF–HFP) + 40 wt % $BMIMBF_4$ + 0.3*M* $LiBF_4$)	1.31	2447	7.85×10^{10}
P(VdF–HFP) + 80 wt % $BMIMBF_4$ + 0.3*M* $LiBF_4$	1.42	1949	5.40×10^{10}

For all of the prepared membranes, temperature-dependent σ measurement was carried out in the wider temperature range from 30 to 160°C. The temperature-dependent σ values of the P(VdF–HFP) plus IL–salt solution gel membranes containing different amounts of IL–salt solution are shown in Figure 11. It is clear from Figure 11 that when the temperature of the polymeric gel membranes was higher, σ was higher. This could be explained as follows. With increasing temperature, more local empty spaces and free volumes for segmental motion were produced; this further facilitated the migration of ions and diminished the effect of ion clouds between the electrode and electrolyte interface. This assisted in the decoupling of ions from the polymer backbone and then facilitated ion transportation within the polymer matrix.

Kim et al.[58] reported a value of σ of about 10^{-2} S/cm at 60°C for IL–polymer gel electrolytes based on IL, ethyl-*N*-methyl morpholinium bis(trifluoromethane sulfonyl)imide, P(VdF–HFP) copolymer, and PC. Hoffman et al.[59] reported an IL-based polymer gel electrolyte for lithium ion batteries with IL, *N*-methyl-*N*-propyl pyrrolidinium bis(trifluoromethyl sulfonyl)azanide, organic carbonates, lithium bis(trifluoromethyl sulfonyl) azanide, and P(VdF–HFP) and found that the σs of the gel electrolytes at room temperature were about 1–2 mS/cm. Although the σ values of the polymer gel electrolyte membranes were significantly higher because of the use of organic carbonates (e.g., EC, PC, vinyl carbonate (VC), diethyl carbonate (DEC)), they always suffer from various kinds of problem, such as flammability, volatility, and electrochemical and thermal instability. Furthermore, because of the presence of IL, the polymer gel electrolyte membranes in this study were thermally stable up to 350–400°C, and these membranes were also nonflammable and nonvolatile; therefore, these electrolytes may be suitable for applications in electrochemical devices at elevated temperatures. Also, σ values up to 160°C were measured for these systems.

The increment in σ with temperature (T) showed an Arrhenius-type thermally activated behavior. However, the σ versus 1/tempertature (T) plot showed significant changes in the values of σ at a temperature that corresponds to the T_m of the polymer, where the amorphous region of the polymer increased considerably. Figure 12 shows the decrease in T_m with increasing concentration of IL–salt solution; this was also discussed earlier in the DSC analysis. The point of inflection (which indicated the T_m of the polymer) drawn from the σ plot was very similar to the T_m obtained by the DSC plots of the P(VdF–HFP) + x wt % IL–salt solution gel membranes (see Figure 12).

σ obeyed Arrhenius behavior at $T < T_m$ and could be expressed as follows:

$$\sigma = \sigma_o \exp(-E_a/kT) \tag{4}$$

where σ_o is the pre-exponential factor, E_a is the activation energy, k is the Boltzmann constant, and T is the temperature (K). The plot between log σ and $1/T$ was used to evaluate E_a, which was found to decrease with increasing concentration of the IL–salt solution in the P(VdF–HFP) polymer. Higher amounts of the IL–salt solution in the polymeric gel membranes increased the plasticization/amorphization of the membranes and assisted in easier ion transport and maintained a good ionic conduction mechanism in the wide temperature range. As far as practical application is concerned, the polymer gel electrolyte membranes so obtained were highly flexible, thermally stable, elastic, and nonvolatile with good σ; other desirable properties appeared to be good enough. These improved properties revealed the basic suitability of polymer gel electrolyte membranes based on ILs for potential applications in Li batteries.

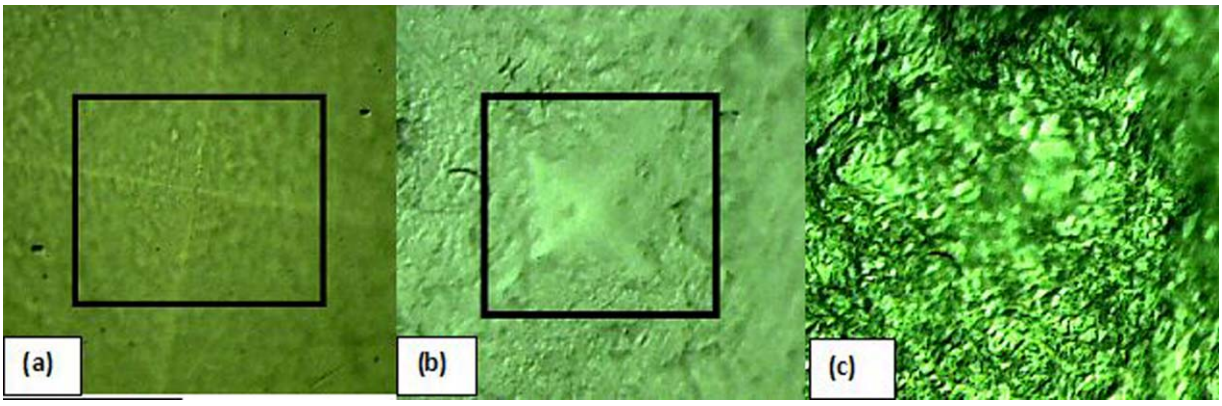

Figure 9. *H* test of the P(VdF–HFP) + x wt % IL–salt solution gel membranes for x = (a) 0, (b) 20, and (c) 80. [Color figure can be viewed in the online issue, which is available at wileyonlinelibrary.com.]

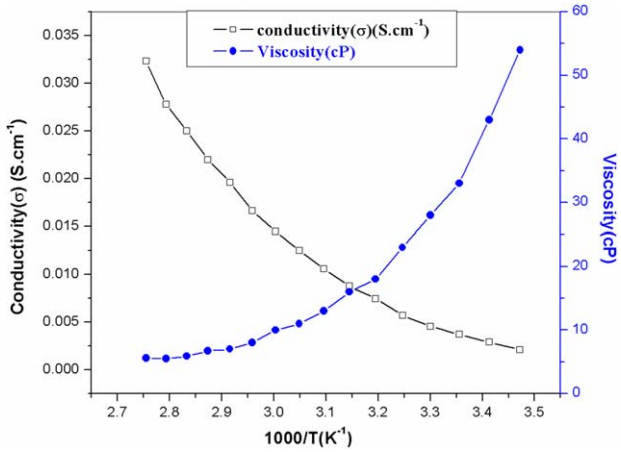

Figure 10. Temperature-dependent σ and viscosity of the pure IL–0.3*M* salt solution. [Color figure can be viewed in the online issue, which is available at wileyonlinelibrary.com.]

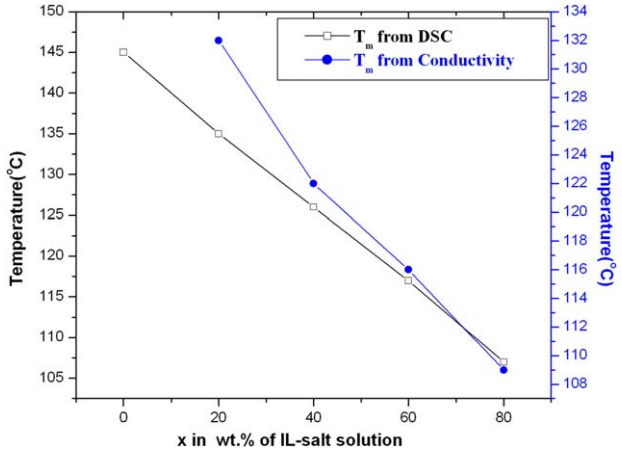

Figure 12. T_m values of the P(VdF–HFP) + x wt % IL–salt solution gel membranes for different values of x obtained by DSC and the point of inflexion in the temperature-dependent σ plot. [Color figure can be viewed in the online issue, which is available at wileyonlinelibrary.com.]

Discussion of the Role of $LiBF_4$ in Controlling the Properties of P(VdF–HFP)–$BMIMBF_4$

Earlier, we reported the thermal, structural, and ionic transport properties of P(VdF–HFP)–$BMIMBF_4$. A comparison of the results of this article with our earlier results[25] was done to help us determine the role of $LiBF_4$. Comparative data of σ are shown in Figure 13 along with X_c values in the inset. Two apparently self-contradictory conclusions, which could be drawn from the data given in Figure 13 with regard to the role of $LiBF_4$, were that the addition of $LiBF_4$ (1) decreased σ and (2) decreased X_c. A more careful and comprehensive look resolved this contradiction. The overall σ depended on the number and mobility of cations and anions. The presence of a peak in the DSC curve at about 107°C (see Figure 4) showed that $LiBF_4$ crystallized out and so did not contribute much to the number of mobile ions. Therefore, the σ change was more likely to be due to the change in the mobility. The decrease in the crystallinity (see inset of Figure 13) enhanced the flexibility of the polymeric chain. The flexibility controlled the hopping conduction because of the complexed cations (Li^+ and $BMIM^+$). The complexation of the former was negligible as $LiBF_4$ crystallized out. $BMIM^+$ was too big an ion to contribute significantly to the hopping conduction. Therefore, it was the BF_4^- anion mobility that was mostly responsible for σ. The motion of anions is known to be more along the translational motion direction. The presence of crystallites of $LiBF_4$ in the path of moving anions may have acted as stumbling blocks and decreased the overall mobility (and, hence, σ, as shown in Figure 13). Because $LiBF_4$ complexed negligibly with the polymer chain, its interaction with the polymer chain should not have affected the thermal stability of the polymer as much as the polymer–IL interaction. These data confirmed this. The T_d

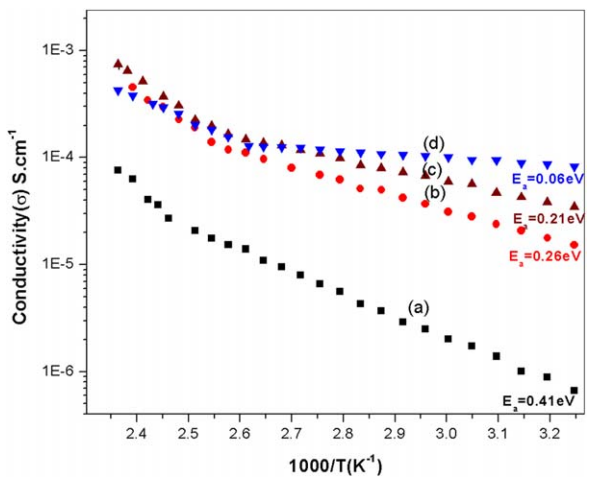

Figure 11. Temperature-dependent σs of the P(VdF–HFP) + x wt % IL–salt solution gel membranes for x = (a) 20, (b) 40, (c) 60, and (d) 80. [Color figure can be viewed in the online issue, which is available at wileyonlinelibrary.com.]

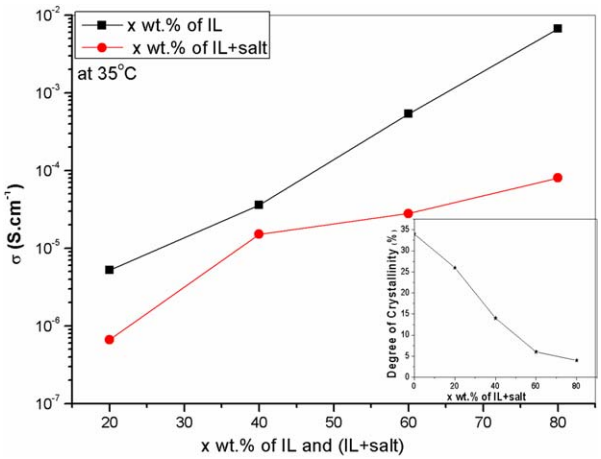

Figure 13. Variation of σ of the P(VdF–HFP) + x wt % IL–salt solution and P(VdF-HFP) + x wt % IL gel membranes at 35°C. The inset shows the variation of X_c of P(VdF–HFP) + x wt % IL–salt solution (where x = 20, 40, 60, and 80). [Color figure can be viewed in the online issue, which is available at wileyonlinelibrary.com.]

Table IV. T_d's of P(VdF–HFP) + *x* wt % (IL + Salt Solution) and P(VdF–HFP) + *x* wt % IL Gel Membranes

	Values of T_d (°C) for	
x	P(VdF-HFP) + x wt % $BMIMBF_4$	P(VdF-HFP) + x wt % $BMIMBF_4$ + $LiBF_4$
0	475	475
20	381	383
40	374	379
60	374 (324[a])	77 (325[a])
80	370 (320[a])	371 (305[a])

[a] Second decomposition peak due to the complexed P(VdF-HFP) given in Figure 5 of this article and Figure 7 of ref. 25.

values of P(VdF–HFP)–$BMIMBF_4$ with and without $LiBF_4$ are given in Table IV.

CONCLUSIONS

Polymer gel electrolyte membranes based on P(VdF–HFP) polymer plus the IL $BMIMBF_4$ plus salt $LiBF_4$ were synthesized and studied. T_m, T_g, X_c, the thermal stability, *E*, and *H* gradually decreased with increasing IL–salt solution concentration in the P(VdF–HFP) polymer, which was still stable enough for practical application. FTIR and DTGA studies showed the simultaneous presence of complexed and uncomplexed ILs in the membrane. From SEM, XRD, and DSC studies, we concluded that the Li salt did not complex well with the P(VdF–HFP) polymer. The σ of the polymer gel electrolyte membrane was found to increase as the amount of IL–salt solution increased in the membranes. The temperature-dependent σ followed an Arrhenius-type thermally activated behavior.

ACKNOWLEDGMENTS

One of the authors (R.K.S.) is grateful to Board of Research in Nuclear Sciences - Department of Atomic Energy (BRNS-DAE), Mumbai, and University Grants Commission (UGC), New Delhi, India, for providing the financial support to carry out this study. Another author Shalu is thankful to UGC, New Delhi, India, for providing a fellowship.

REFERENCES

1. Scrosati, B. Applications of Electroactive Polymers; Chapman & Hall: London, **1993**.
2. Nishi, Y.; Schalkwijk, W. V.; Scrosati, B. In Advances in Li-Ion Batteries; Kluwer Academic/Plenum: New York, **2002**; Chapter 7.
3. Lee, J. S.; Quan, N. D.; Huang, J. M.; Lee, S. D.; Kim, H.; Lee, H.; Kim, H. S. *J. Ind. Eng. Chem.* **2006**, *12*, 175.
4. Sekhon, S. S.; Kaur, D. P.; Park, J. S.; Yamada, K. *Electrochim. Acta* **2012**, *60*, 366.
5. Byrne, N.; Efthimiadis, J.; MacFarlane, D. R.; Forsyth, M. *J. Mater. Chem.* **2004**, *14*, 127.
6. Tarascon, J. M.; Gozdz, A. S.; Schmutz, C.; Shokoohi, F.; Warren, P. C. Performance of Bellcore's plastic rechargeable Li-ion batteries. *Solid State Ionics* **1996**, *86–88*, 49.
7. Tian, X.; Zhu, B.; Xu, Y. *J. Membr. Sci.* **2005**, *248*, 109.
8. Ramesh, S.; Lu, S. C. *J. Mol. Struct.* **2011**, *994*, 403.
9. Lim, D. H.; Manuel, J.; Ahn, J. H.; Kim, J. K.; Jacobsson, P.; Matic, A.; Ha, J. K.; Cho, K. K.; Kim, K. W. *Solid State Ionics* **2012**, *225*, 631.
10. Pandey, G. P.; Agrawal, R. C.; Hashmi, S. A. *J. Power Sources* **2009**, *190*, 563.
11. Asmara, S. N.; Kufian, M. Z.; Majid, S. R.; Arof, A. K. *Electrochim. Acta* **2011**, *57*, 91.
12. Stallworth, P. E.; Greenbaum, S. G.; Croce, F.; Slanet, S.; Salomon, M. *Electrochim. Acta* **1995**, *40*, 2137.
13. Chaurasia, S. K.; Singh, R. K.; Chandra, S. *J. Raman Spectrosc.* **2011**, *42*, 2168.
14. Martinelli, A.; Matic, A.; Jacobsson, P.; Borjesson, L.; Fernicola, A.; Panero, S.; Scrosati, B.; Ohno, H. *J. Phys. Chem. B* **2007**, *111*, 12462.
15. Tsunemi, K.; Ohno, H.; Tsuchida, E. *Electrochim. Acta* **1983**, *28*, 833.
16. Ohno, H. *Macromol. Symp.* **2007**, *249–250*, 551.
17. Noda, A.; Hayamizu, K.; Watanabe, M. *J. Phys. Chem. B* **2001**, *105*, 4603.
18. Chaurasia, S. K.; Singh, R. K.; Chandra, S. *J. Polym. Sci. Part B: Polym. Phys.* **2011**, *49*, 291.
19. Ohno, H. Electrochemical Aspects of Ionic Liquids; Wiley: Hoboken, NJ, **2005**.
20. Seki, S.; Susan, M. A. B. H.; Kaneko,; Tokuda, T. H.; Noda, A.; Watanabe, M. *J. Phys. Chem. B* **2005**, *109*, 3886.
21. Jansen, J. C.; Friess, K.; Clarizia, G.; Schauer, J.; Izak, P. *Macromolecules* **2011**, *44*, 39.
22. Chaurasia, S. K.; Singh, R. K.; Chandra, S. *Solid State Ionics* **2011**, *183*, 32.
23. Ye, H.; Huang, J.; Xu, J. J.; Khalfan, A.; Greenbaum, S. G. *J. Electrochem. Soc.* **2007**, *21*, A1048.
24. Brandt, K. *Solid State Ionics* **1994**, *69*, 173.
25. Yang, P.; Liu, L.; Li, L.; Hou, J.; Xu, Y.; Ren, X.; An, M.; Li, N. *Electrochim. Acta* **2014**, *115*, 454.
26. Navarra, M. A.; Manzi, J.; Lombardo, L.; Panero, S.; Scrosati, B. *ChemSusChem* **2011**, *4*, 125.
27. Jung, K.-N.; Lee, J.-I.; Jung, J.-H.; Shin, K.-H.; Lee, J.-W. *Chem. Commun.* **2014**, *50*, 5458.
28. Shalu.; Chaurasia, S. K.; Singh, R. K.; Chandra, S. *J. Phys. Chem. B* **2013**, *117*, 897.
29. Abbrent, S.; Plestil, J.; Hlavata, D.; Lindgren, J.; Tegenfeldt, J.; Wendsjo, A. *Polymer* **2001**, *42*, 1407.
30. Saikia, D.; Kumar, A. *Electrochim. Acta* **2004**, *49*, 2581.
31. Saikia, D.; Han, C. C.; Chen-Yang, Y. W. *J. Power Sources* **2008**, *185*, 570.
32. Fahmi, E. M.; Ahmad, A.; Nazeri, N. N. M.; Hamzah, H.; Razali, H.; Rahman, M. Y. A. *Int. J. Electrochem. Sci.* **2012**, *7*, 5798.

33. Jin, J.; Wen, Z.; Liang, X.; Cui, Y.; Wu, X. *Solid State Ionics* **2012**, *225*, 604.
34. Scott, M. P.; Brazel, C. S.; Benton, M. G.; Mays, J. W.; Holbrey, J. D.; Rogers, R. D. *Chem. Commun.* **2002**, 1370.
35. Reynhardt, E. C.; Lourens, J. A. J. *J. Chem. Phys.* **1984**, *80*, 6240.
36. Joost, M.; Kunze, M.; Jeong, S.; Schönhoff, M.; Wintera, M.; Passerini, S. *Electrochim. Acta* **2012**, *86*, 330.
37. Liew, C.-W.; Ong, Y. S.; Lim, J. Y.; Lim, C. S.; Teoh, K. H.; Ramesh, S. *Int. J. Electrochem. Sci.* **2013**, *8*, 7779.
38. Tian, X.; Jiang, X.; Zhu, B.; Xu, Y. *J. Membr. Sci.* **2006**, *279*, 479.
39. Kobayashi, M.; Tashiro, K.; Tadokoro, H. *Macromolecules* **1975**, *8*, 158.
40. Li, Z.; Su, G.; Gao, D.; Wang, X.; Li, X. *Electrochim. Acta* **2004**, *49*, 4633.
41. Pandey, G. P.; Hashmi, S. A. *J. Power Sources* **2009**, *187*, 627.
42. Heimer, N. E.; Sesto, R. E. D.; Meng, Z.; Wilkes, J. S.; Robert, W.; Carper, J. *Mol. Liq.* **2006**, *124*, 84.
43. Shi, J.; Wu, P.; Yan, F. *Langmuir* **2010**, *26*, 11427.
44. Jeon, Y.; Sung, J.; Seo, C.; Lim, H.; Cheong, H.; Kang, M.; Moon, B.; Ouchi, Y.; Kim, D. *J. Phys. Chem. B* **2008**, *112*, 4735.
45. Gonfa, G.; Bustam, M. A.; Man, Z.; Abdul Mutalib, M. I. *Asian Trans. Eng.* **2011**, *1*, 24.
46. Hunt, P. A.; Kirchner, B.; Welton, T. *Chem. Eur. J.* **2006**, *12*, 6762.
47. Kempter, V. *J. Mol. Struct.* **2010**, *972*, 22.
48. Izgorodina, E. I.; Maganti, R.; Armel, V.; Dean, P. M.; Pringle, J. M.; Seddon, K. R.; MacFarlane, D. R. *J. Phys. Chem. B* **2011**, *115*, 14688.
49. Izgorodina, E. I.; MacFarlane, D. R. *J. Phys. Chem. B* **2011**, *115*, 14659.
50. Baltá-Calleja, F. J.; Martinez-Salazar, J.; Rueda, D. R. In Encyclopedia of Polymer Science and Engineering; Kroschwitz, J. I., Ed.; Wiley: New York, **1987**; Vol. *7*, p 614.
51. Benavente, R.; Pérez, E.; Quijada, R. *J. Polym. Sci. Polym. Phys.* **2001**, *39*, 277.
52. Sacristán, J.; Benavente, R.; Pereña, J. M.; Pérez, E.; Bello, A.; Rojas, R.; Quijada, R.; Rabagliati, F. M. *J. Therm. Anal. Calorim.* **1999**, *58*, 559.
53. Flores, A.; Baltá-Calleja, F. J.; Attenburrow, G. E.; Basset, D. C. *Polymer* **2000**, *41*, 5431.
54. Boycheva, S. V.; Vassilev, V. S.; Petkov, P. *J. Optoelectron. Adv. Mater.* **2001**, *3*, 503.
55. Salminen, J.; Prausnitza, J. M.; Newman, J. Preliminary Report, Sept. 21, 2005, Department of Chemical Engineering, University of California, Berkeley, CA 94720; USA Environmental Energy Technology Division, LBNL: Berkeley, CA, and USA Chemical Sciences Division, LBNL: Berkeley, CA.
56. Kumar, Y.; Pandey, G. P.; Hashmi, S. A. *J. Phys. Chem. C* **2012**, *116*, 26118.
57. Kim, K. S.; Park, S. Y.; Choi, S.; Lee, H. *J. Power Sources* **2006**, *155*, 385.
58. Hofmann, A.; Schulz, M.; Hanemann, T. *Electrochim. Acta* **2013**, *89*, 823.
59. Grey, F. M. Solid Polymer Electrolytes: Fundamental and Technological Applications; VCH: New York, **1991**.